DETECTING EDGES OF REFLECTIONS FROM A SINGLE IMAGE VIA CONVEX OPTIMIZATION

Katsuhiro TOYOKAWA, Shunsuke ONO, Masao YAMAGISHI, and Isao YAMADA

Dept. of Communications and Computer Engineering, Tokyo Institute of Technology
E-mail: {toyokawa, ono, myamagi, isao}@sp.ce.titech.ac.jp

ABSTRACT

We propose to detect edges of reflections, which we call the *REF-edges*, from a single image via convex optimization. Our method is designed based on two observations on reflections: (i) reflections have almost monotone color and (ii) color around REF-edges varies smoothly. The first one can be translated into the property that gradients around REF-edges distribute linearly in the RGB color space, which we call the *REF-linearity*. The second one can be interpreted as follows: *color differences* around REF-edges are small; for an entry of REF-edges, gradients among its surrounding entries have small variance. Using the above properties, we characterize REF-edges as a solution of a constrained convex optimization problem. The optimization problem is solved by the Alternating Direction Method of Multipliers (ADMM). Experiments using real-world images with reflections show the utility of our proposed method.

Index Terms— Reflection detection, edge detection, REF-linearity, color difference, ADMM

1. INTRODUCTION

Images with reflections are often acquired in everyday life when one takes pictures through transparent glass. Since such reflections degrade application performance as well as visual quality, reflection detection is a key process in various image processing applications, including reflection removal (e.g. [1–5]), image classification/recognition, and object detection (e.g. [6]). In particular, for precision of object detection, edges of reflections are required to be distinguished from those of objects desired to be detected. With this background, reflection detection using multiple/sequential images has been studied in, e.g., [7, 8]. However, in the case where only a single image is given, reflection detection becomes much more challenging and, to the best of our knowledge, has not been reported yet.

One of the most important features of reflections is edges of reflections, which we call the *REF-edges*, because they give us many pieces of information, including shape, size, and location. Actually, in the work of Levin et al. [3], REF-edges marked manually have been utilized to realize reflection removal. Therefore, an automatic detection of REF-edges from a single image has been demanded.

In this paper, we propose to detect REF-edges from a single image via convex optimization. Suppose that a given color image $\mathbf{U}_{\mathrm{gvn}}$ can be decomposed into $\mathbf{U}_{\mathrm{gvn}} = \mathbf{U}_{\mathrm{scn}} + \mathbf{U}_{\mathrm{ref}}$, where $\mathbf{U}_{\mathrm{scn}}$ and $\mathbf{U}_{\mathrm{ref}}$ are the scene and reflection image, respectively. The proposed method extracts REF-edges based on the following two observations on reflections in real-world images (see Fig. 1 (a) and Fig. 3 (a), (e)):

A1. Reflections have almost monotone color.

A2. Color around REF-edges varies smoothly.

To leverage these observations in our proposed method, we first translate them into mathematical criteria. Specifically, the observation A1 can be viewed as the linearity of the distribution of gradients around REF-edges in the RGB color space (Fig. 1 (c)), which we call the *REF-linearity*. By constructing a certain matrix based on the gradients, the property is then reduced to the low-rankness of the matrix. Thus, promoting the low-rankness of the matrix well characterizes the true REF-edge image. The observation A2 tells us the two properties: (i) in the L*a*b* color space, *color differences*[1] around REF-edges are small (Fig. 1 (d)); (ii) when we focus on an entry of REF-edges, gradients among its surrounding entries have small variance (see their histograms in Fig. 1 (e)). These properties imply that we can expect to approximate the true REF-edge image by removing entries of large color differences and variances. Based on the above interpretations, we formulate an REF-edge estimation as a constrained convex optimization problem, and solve it by the *Alternating Direction Method of Multipliers* (ADMM) [9]. Experimental results using real-world images with reflections illustrate the utility of the proposed method.

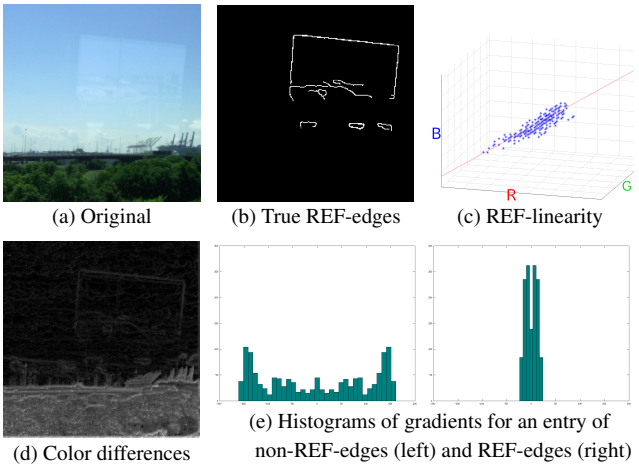

(a) Original (b) True REF-edges (c) REF-linearity

(d) Color differences (e) Histograms of gradients for an entry of non-REF-edges (left) and REF-edges (right)

Fig. 1: Three properties of REF-edges (the REF-linearity, small color differences, and small variance of the histogram): The proposed method is designed based on these properties.

We would like to thank the anonymous reviewers for their helpful comments. This work was supported in part by JSPS Grants-in-Aid (24-2522, 24800022, B-21300091).

[1]The L*a*b* color space is designed to approximate human vision. The color difference between two colors (L_1^*, a_1^*, b_1^*) and (L_2^*, a_2^*, b_2^*) is defined by $\sqrt{(L_1^* - L_2^*)^2 + (a_1^* - a_2^*)^2 + (b_1^* - b_2^*)^2}$.

978-1-4799-2893-4/14/$31.00 ©2014 IEEE

2. PRELIMINARIES

Let $\mathbb{R}$, $\mathbb{R}_+$, $\mathbb{R}_{++}$, and $\mathbb{N}$ be the sets of all real numbers, non-negative real numbers, positive real numbers, and positive integers, respectively. We use boldface capital and small letters to denote matrices and vectors, respectively. Moreover, we express a color image $\mathbf{U} \in \mathbb{R}^{n_v \times n_h \times 3}$ $(n_v, n_h \in \mathbb{N})$ as $\mathbf{U} = \big(\mathbf{U}^{(1)}, \mathbf{U}^{(2)}, \mathbf{U}^{(3)}\big)$, where $\mathbf{U}^{(p)} \in \mathbb{R}^{n_v \times n_h}$ $(p = 1, 2, 3)$ denote each RGB channel of $\mathbf{U}$, and $N = n_v n_h$ is the number of the entries in each RGB channel. The (i, j)-th entry is denoted by $(\cdot)_{i,j}$. Let Δ_{v_+}, Δ_{h_-}, $\Delta_{v_+h_-}$, and $\Delta_{v_+h_+}$ be the vertical, horizontal, and two diagonal discrete gradient linear operators with Neumann boundary.

2.1. Nuclear norm

We will use the *nuclear norm*, known as a convex envelope of the rank of a matrix [10], in our optimization. It is defined, for matrices of size $4N \times 3$, as follows: $\|\cdot\|_*\colon \mathbb{R}^{4N\times 3} \to \mathbb{R}_+ : \mathbf{M} \mapsto \sum_{p=1}^{3} s_p(\mathbf{M})$, where $s_p(\cdot)$ is the p-th largest singular value of $(\cdot)$. We denote the singular value decomposition of $\mathbf{M} \in \mathbb{R}^{4N\times 3}$ as the matrix $\mathbf{M} = \mathbf{P}\mathbf{\Sigma}\mathbf{Q}^\top$, where $\mathbf{P} \in \mathbb{R}^{4N\times 4N}$, $\mathbf{Q} \in \mathbb{R}^{3\times 3}$ are orthogonal matrices, and $\mathbf{\Sigma} \in \mathbb{R}^{4N\times 3}$ contains the singular values on its main diagonal and 0's elsewhere ($(\cdot)^\top$ stands for the transposition).

2.2. Alternating Direction Method of Multipliers (ADMM)

The Alternating Direction Method of Multipliers (ADMM) [9] can solve the following convex optimization problem:

$$\underset{\mathbf{X}\in\mathcal{X}}{\text{minimize}}\; f(\mathbf{X}) + g\big(\Lambda(\mathbf{X})\big), \tag{1}$$

where $f : \mathcal{X} \to (-\infty, \infty]$ and $g : \mathcal{Y} \to (-\infty, \infty]$ are proper lower semicontinuous convex functions, and $\Lambda : \mathcal{X} \to \mathcal{Y}$ is a linear operator ($\mathcal{X}$ and $\mathcal{Y}$ stand for *real Hilbert spaces* with the standard inner product $\langle\cdot,\cdot\rangle$ and its induced norm $\|\cdot\|$). The ADMM iteratively computes the following steps:

$$\mathbf{X}^{(k+1)} = \arg\min_{\mathbf{X}\in\mathcal{X}} f(\mathbf{X}) + \tfrac{\rho}{2}\|\Lambda(\mathbf{X}) - \mathbf{Y}^{(k)} + \tfrac{1}{\rho}\mathbf{\Theta}^{(k)}\|^2, \tag{2}$$

$$\mathbf{Y}^{(k+1)} = \operatorname{prox}_{\rho^{-1}g}\big(\Lambda(\mathbf{X}^{(k+1)}) + \tfrac{1}{\rho}\mathbf{\Theta}^{(k)}\big), \tag{3}$$

$$\mathbf{\Theta}^{(k+1)} = \mathbf{\Theta}^{(k)} + \rho\big(\Lambda(\mathbf{X}^{(k+1)}) - \mathbf{Y}^{(k+1)}\big),$$

where $\rho \in \mathbb{R}_{++}$ and $\operatorname{prox}_{\rho^{-1}g}$ denotes the *proximity operator*[2] of g. The convergence of the ADMM has been studied by, e.g., Eckstein and Bertekas [11].

3. PROPOSED METHOD

We propose an REF-edge detection method based on convex optimization whose action is illustrated in Fig. 2. First, applying an existing edge detector to a given color image with reflections $\mathbf{U}_{\text{gvn}} \in \mathbb{R}^{n_v\times n_h\times 3}$, we obtain an initial edge image $\mathbf{E}_{\text{gvn}} \in \{0,1\}^{n_v\times n_h}$. Next, we extract REF-edges from the initial edge image $\mathbf{E}_{\text{gvn}}$ by solving a certain convex optimization problem. Finally, the extracted REF-edge image is binarized by a simple thresholding operation. In what follows, we elaborate on the key step of the proposed method, i.e., the optimization.

[2]For any $\gamma \in \mathbb{R}_{++}$, the proximity operator of a proper lower semicontinuous convex function f on $\mathcal{X}$ is given by $\operatorname{prox}_{\gamma f}(\mathbf{X}) := \arg\min_{\mathbf{Y}\in\mathcal{X}}\big\{f(\mathbf{Y}) + \frac{1}{2\gamma}\|\mathbf{X}-\mathbf{Y}\|^2\big\}$.

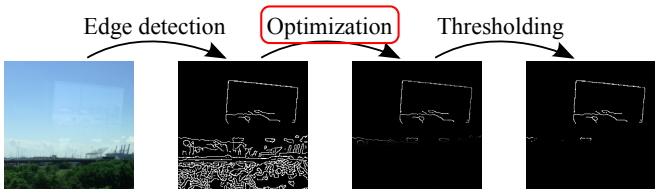

Fig. 2: The flowchart in the proposed REF-edge detection.

3.1. Formulation

For an initial edge image $\mathbf{E}_{\text{gvn}}$, we estimate an REF-edge image by solving the following convex optimization:[3]

$$\underset{\mathbf{E}\in C_{[0,1]}^{\mathbf{E}_{\text{gvn}}}\cap C_{\varepsilon}^{\mathbf{E}_{\text{gvn}}}}{\text{minimize}}\; \|\Phi(\mathbf{E})\|_* + \tfrac{\lambda_1}{2}\|\Omega_{\text{L*a*b*}}(\mathbf{E})\|_F^2 + \tfrac{\lambda_2}{2}\|\Omega_{\text{var}}(\mathbf{E})\|_F^2, \tag{4}$$

where the first term is designed to promote the REF-linearity, the second term to remove entries of large color differences, the third term to eliminate entries of large variance, and the constraints express the fidelity regarding $\mathbf{E}_{\text{gvn}}$. Detailed explanations are given below.

3.1.1. The first term in (4)

To exploit the REF-linearity in the estimation, we translate it into the low rankness of a certain matrix, which we call the *RGB-gradient matrix*, defined as follows. Let $\mathbf{D}_{v_+}^{(\mathbf{U}_{\text{gvn}},\mathbf{E})} \in \mathbb{R}^{N\times 3}$ be the matrix defined by using $\mathbf{E} \in \mathbb{R}^{n_v\times n_h}$, i.e.,

$$\mathbf{D}_{v_+}^{(\mathbf{U}_{\text{gvn}},\mathbf{E})} := \Big[\mathbf{d}_{v_+}^{(\mathbf{U}_{\text{gvn}}^{(1)},\mathbf{E})}\, \mathbf{d}_{v_+}^{(\mathbf{U}_{\text{gvn}}^{(2)},\mathbf{E})}\, \mathbf{d}_{v_+}^{(\mathbf{U}_{\text{gvn}}^{(3)},\mathbf{E})}\Big] \in \mathbb{R}^{N\times 3},$$

where $\mathbf{d}_{v_+}^{(\mathbf{U}_{\text{gvn}}^{(p)},\mathbf{E})} := \operatorname{vec}\big(\Delta_{v_+}(\mathbf{U}_{\text{gvn}}^{(p)}) \circledast \mathbf{E}\big) \in \mathbb{R}^N$ $(p = 1, 2, 3)$. Here, the entry-wise multiplication between $\mathbf{X}$ and $\mathbf{Y}$ is defined by $(\mathbf{X} \circledast \mathbf{Y})_{i,j} := (\mathbf{X})_{i,j}(\mathbf{Y})_{i,j}$, and the linear operator $\operatorname{vec}(\cdot)$ maps a matrix $[\mathbf{x}_1\, \mathbf{x}_2\, \ldots\, \mathbf{x}_{n_h}] \in \mathbb{R}^{n_v\times n_h}$ to the corresponding vector $[\mathbf{x}_1^\top\, \mathbf{x}_2^\top\, \ldots\, \mathbf{x}_{n_h}^\top]^\top \in \mathbb{R}^N$. The matrices $\mathbf{D}_{h_+}^{(\mathbf{U}_{\text{gvn}},\mathbf{E})}$, $\mathbf{D}_{v_+h_-}^{(\mathbf{U}_{\text{gvn}},\mathbf{E})}$, and $\mathbf{D}_{v_+h_+}^{(\mathbf{U}_{\text{gvn}},\mathbf{E})}$ are constructed in a similar way. The RGB-gradient matrix is then defined by $\Phi(\mathbf{E})$, where

$$\Phi : \mathbb{R}^{n_v\times n_h} \to \mathbb{R}^{4N\times 3} : \mathbf{E} \mapsto \begin{bmatrix} \mathbf{D}_{v_+}^{(\mathbf{U}_{\text{gvn}},\mathbf{E})} \\ \mathbf{D}_{h_+}^{(\mathbf{U}_{\text{gvn}},\mathbf{E})} \\ \mathbf{D}_{v_+h_-}^{(\mathbf{U}_{\text{gvn}},\mathbf{E})} \\ \mathbf{D}_{v_+h_+}^{(\mathbf{U}_{\text{gvn}},\mathbf{E})} \end{bmatrix}.$$

If $\mathbf{E}$ is the true REF-edge image, the rank of the RGB-gradient matrix is low because its column vectors are linearly dependent. Hence, suppressing the nuclear norm of the RGB-gradient matrix leads to an efficient promotion of the REF-linearity (similar translation of linearity into low-rankness is adopted in [12]).

3.1.2. The second term in (4)

To extract entries of small color differences, we assign large weight to entries corresponding to large color differences, which results in removing entries of large weight via minimization of (4). To do so, we introduce a weight matrix $\mathbf{W}_{\text{L*a*b*}} \in \mathbb{R}_+^{n_v\times n_h}$ whose (i, j)-th entry is defined by the sum of its surrounding entries of total color differences of four directions normalized so that max

[3]For a matrix $\mathbf{X} \in \mathbb{R}^{m\times n}$ $(m, n \in \mathbb{N})$, the *Frobenius norm* is defined by $\|\mathbf{X}\|_F := \sqrt{\sum_{i,j} |(\mathbf{X})_{i,j}|^2}$.

value of all entries is 1. More precisely, the total color differences is $\mathbf{C}^{(\mathbf{U}_{\mathrm{gvn}})} := \mathbf{C}_{v_+}^{(\mathbf{U}_{\mathrm{gvn}})} + \mathbf{C}_{h_+}^{(\mathbf{U}_{\mathrm{gvn}})} + \mathbf{C}_{v_+h_-}^{(\mathbf{U}_{\mathrm{gvn}})} + \mathbf{C}_{v_+h_+}^{(\mathbf{U}_{\mathrm{gvn}})} \in \mathbb{R}_+^{n_v \times n_h}$, where $\left(\mathbf{C}_{\bullet}^{(\mathbf{U}_{\mathrm{gvn}})}\right)_{i,j} := \left(\sum_{p=1}^{3}\left(\Delta_{\bullet}(\widehat{\mathbf{U}}_{\mathrm{gvn}}^{(p)})\right)_{i,j}^2\right)^{\frac{1}{2}}$ for any $\bullet \in \{v_+, h_+, v_+h_-, v_+h_+\}$ and $\widehat{\mathbf{U}}_{\mathrm{gvn}} := (\widehat{\mathbf{U}}_{\mathrm{gvn}}^{(1)}, \widehat{\mathbf{U}}_{\mathrm{gvn}}^{(2)}, \widehat{\mathbf{U}}_{\mathrm{gvn}}^{(3)}) \in \mathbb{R}^{n_v \times n_h \times 3}$ is an L*a*b* color image transformed from a given RGB color image $\mathbf{U}_{\mathrm{gvn}}$; and when we focus on an entry, its weight is the normalized sum of its surrounding entries of the total color differences, i.e., $(\mathbf{W}_{\mathrm{L^*a^*b^*}})_{i,j} := \frac{1}{m_{\mathrm{L^*a^*b^*}}} \sum_{(i_1,j_1)\in\mathcal{I}_{i,j}} (\mathbf{C}^{(\mathbf{U}_{\mathrm{gvn}})})_{i_1,j_1}$, where $m_{\mathrm{L^*a^*b^*}} := \max_{i,j} \sum_{(i_1,j_1)\in\mathcal{I}_{i,j}} (\mathbf{C}^{(\mathbf{U}_{\mathrm{gvn}})})_{i_1,j_1}$ and $\mathcal{I}_{i,j}$ denotes an index set of the (i_1, j_1)-th entries in an area of a certain radius r, which depends on the size of an image, around the (i, j)-th entry. Finally, the second term in (4) is designed as the Frobenius norm of $\Omega_{\mathrm{L^*a^*b^*}}(\mathbf{E})$, where

$$\Omega_{\mathrm{L^*a^*b^*}} : \mathbb{R}^{n_v \times n_h} \to \mathbb{R}^{n_v \times n_h} : \mathbf{E} \mapsto \mathbf{W}_{\mathrm{L^*a^*b^*}} \circledast \mathbf{E}.$$

A2 implies that if $\mathbf{E}$ is the true REF-edge image, the magnitude of $\Omega_{\mathrm{L^*a^*b^*}}(\mathbf{E})$ is small. Hence, suppressing the Frobenius norm of $\Omega_{\mathrm{L^*a^*b^*}}(\mathbf{E})$ is expected to remove non-REF-edges from $\mathbf{E}_{\mathrm{gvn}}$.

3.1.3. The third term in (4)

Similarly to the second term, we eliminate entries of large variance of gradients by assigning large weights. For this purpose, we construct a weight matrix $\mathbf{W}_{\mathrm{var}} \in \mathbb{R}_+^{n_v \times n_h}$ whose (i, j)-th entry is defined by the sum of its surrounding entries of total RGB variance normalized so that maximum value of all entries becomes 1. In detail, the total RGB variance is $\mathbf{V}^{(\mathbf{U}_{\mathrm{gvn}})} := \sum_{p=1}^{3} \mathbf{V}^{(\mathbf{U}_{\mathrm{gvn}}^{(p)})} \in \mathbb{R}_+^{n_v \times n_h}$, where $(\mathbf{V}^{(\mathbf{U}_{\mathrm{gvn}}^{(p)})})_{i,j}$ equals the variance[4] of (i, j)-th gradient data set $\delta_{i,j}^{(p)} := \left\{ \left((\mathbf{U}_{\mathrm{gvn}}^{(p)})_{i_1,j_1} - (\mathbf{U}_{\mathrm{gvn}}^{(p)})_{i_2,j_2}\right)_{i_1,j_1} \in \mathbb{R} \;\middle|\; (i_1, j_1) \in \mathcal{I}_{i,j} \right\}$ and the (i_1, j_1)-th and (i_2, j_2)-th entries are symmetrical with respect to the (i, j)-th entry; and weight of each entry is defined by the normalized sum of its surrounding entries of the total RGB variance, i.e., $(\mathbf{W}_{\mathrm{var}})_{i,j} := \frac{1}{m_{\mathrm{var}}} \sum_{(i_1,j_1)\in\mathcal{I}_{i,j}} (\mathbf{V}^{(\mathbf{U}_{\mathrm{gvn}})})_{i_1,j_1}$, where $m_{\mathrm{var}} := \max_{i,j} \sum_{(i_1,j_1)\in\mathcal{I}_{i,j}} (\mathbf{V}^{(\mathbf{U}_{\mathrm{gvn}})})_{i_1,j_1}$. In final, the third term is designed as the Frobenius norm of $\Omega_{\mathrm{var}}(\mathbf{E})$, where

$$\Omega_{\mathrm{var}} : \mathbb{R}^{n_v \times n_h} \to \mathbb{R}^{n_v \times n_h} : \mathbf{E} \mapsto \mathbf{W}_{\mathrm{var}} \circledast \mathbf{E}.$$

Again, provided that $\mathbf{E}$ is the true REF-edge image, the magnitude of $\Omega_{\mathrm{var}}(\mathbf{E})$ is small. Therefore, suppressing the Frobenius norm of $\Omega_{\mathrm{var}}(\mathbf{E})$ gives a good estimate of the true REF-edge image.

3.1.4. The constraints in (4)

Since an initial edge image $\mathbf{E}_{\mathrm{gvn}}$ contains REF-edges, the estimated REF-edge image should satisfy the following constraints:

$$C_{[0,1]}^{\mathbf{E}_{\mathrm{gvn}}} := \left\{ \mathbf{E} \in \mathbb{R}^{n_v \times n_h} \;\middle|\; \begin{array}{ll} (\mathbf{E})_{i,j} = 0 & \text{if } (\mathbf{E}_{\mathrm{gvn}})_{i,j} = 0 \\ (\mathbf{E})_{i,j} \in [0,1] & \text{if } (\mathbf{E}_{\mathrm{gvn}})_{i,j} = 1 \end{array} \right\}, \tag{5}$$

$$C_{\varepsilon}^{\mathbf{E}_{\mathrm{gvn}}} := \left\{ \mathbf{E} \in \mathbb{R}^{n_v \times n_h} \;\middle|\; \|\mathbf{E} - \mathbf{E}_{\mathrm{gvn}}\|_1 := \textstyle\sum_{i,j} |(\mathbf{E} - \mathbf{E}_{\mathrm{gvn}})_{i,j}| \le \varepsilon \right\},$$

where $\varepsilon \in \mathbb{R}_{++}$ is selected based on the number of non-REF-edges. The constraint $C_{[0,1]}^{\mathbf{E}_{\mathrm{gvn}}}$ expresses that entries detected as edges in $\mathbf{E}_{\mathrm{gvn}}$ are only allowed to become REF-edges. Meanwhile, the constraint $C_{\varepsilon}^{\mathbf{E}_{\mathrm{gvn}}}$ represents the ℓ_1-norm fidelity to $\mathbf{E}_{\mathrm{gvn}}$. This is because entries corresponding to non-REF-edges in $\mathbf{E}_{\mathrm{gvn}}$ can be seen as an impulsive noise added to the true REF-edge image. Note that the ℓ_1-norm is widely recognized as a robust fidelity measure for an impulsive noise contamination.

[4]The variance of (i, j)-th gradient data set $\delta_{i,j}^{(p)}$ is defined by $\sigma^2(\delta_{i,j}^{(p)}) := \frac{1}{|\mathcal{I}_{i,j}|} \sum_{x_{i_1,j_1} \in \delta_{i,j}^{(p)}} (x_{i_1,j_1} - \overline{x}_{i,j})^2$, where $|\mathcal{I}_{i,j}|$ is the cardinality of $\mathcal{I}_{i,j}$ and $\overline{x}_{i,j} := \frac{1}{|\mathcal{I}_{i,j}|} \sum_{x_{i_1,j_1} \in \delta_{i,j}^{(p)}} x_{i_1,j_1}$.

Algorithm 1 Solver for the problem in (6)

Get $\mathbf{E}_{\mathrm{gvn}}$. Set $k = 0$ and $\mathbf{E}^{(0)} = \mathbf{E}_{\mathrm{gvn}}$. Choose $\varepsilon, \rho \in \mathbb{R}_{++}$.
$\mathbf{Y}_1^{(0)} \leftarrow \Phi(\mathbf{E}^{(0)})$, $\mathbf{Y}_2^{(0)} \leftarrow \mathbf{E}^{(0)}$, $\mathbf{\Theta}_1^{(0)} \leftarrow \Phi(\mathbf{E}^{(0)})$, $\mathbf{\Theta}_2^{(0)} \leftarrow \mathbf{E}^{(0)}$.
while a stop criterion is not satisfied **do**
  $\mathbf{E}^{(k+1)} \leftarrow P_{C_{[0,1]}^{\mathbf{E}_{\mathrm{gvn}}}}\Big(\big(\Omega^* \circ \Omega + \rho(\Phi^* \circ \Phi + I^* \circ I)\big)^{-1}$
    $\big(\Phi^*(\rho\mathbf{Y}_1^{(k)} - \mathbf{\Theta}_1^{(k)}) + (\rho\mathbf{Y}_2^{(k)} - \mathbf{\Theta}_2^{(k)})\big)\Big)$.
  $\mathbf{Y}_1^{(k+1)} \leftarrow \mathrm{prox}_{\rho^{-1}\|\cdot\|_*}\big(\Phi(\mathbf{E}^{(k+1)}) + \frac{1}{\rho}\mathbf{\Theta}_1^{(k)}\big)$.
  $\mathbf{Y}_2^{(k+1)} \leftarrow P_{C_{\varepsilon}^{\mathbf{E}_{\mathrm{gvn}}}}\big(\mathbf{E}^{(k+1)} + \frac{1}{\rho}\mathbf{\Theta}_2^{(k)}\big)$.
  $\mathbf{\Theta}_1^{(k+1)} \leftarrow \mathbf{\Theta}_1^{(k)} + \rho\big(\Phi(\mathbf{E}^{(k+1)}) - \mathbf{Y}_1^{(k+1)}\big)$.
  $\mathbf{\Theta}_2^{(k+1)} \leftarrow \mathbf{\Theta}_2^{(k)} + \rho\big(\mathbf{E}^{(k+1)} - \mathbf{Y}_2^{(k+1)}\big)$.
  $k \leftarrow k + 1$.
end while
Output $\mathbf{E}^{(k)}$.

3.2. Solver

We provide an efficient algorithmic solution to (4) by applying the ADMM. First, (4) is rewritten as

$$\underset{\mathbf{E}\in\mathbb{R}^{n_v\times n_h}}{\text{minimize}} \; \tfrac{1}{2}\|\Omega(\mathbf{E})\|_F^2 + \iota_{C_{[0,1]}^{\mathbf{E}_{\mathrm{gvn}}}}(\mathbf{E}) + \|\Phi(\mathbf{E})\|_* + \iota_{C_{\varepsilon}^{\mathbf{E}_{\mathrm{gvn}}}}(\mathbf{E}), \tag{6}$$

where the linear operator $\Omega : \mathbb{R}^{n_v \times n_h} \to \mathbb{R}^{n_v \times n_h}$ is defined by

$$\Omega : (\mathbf{E})_{i,j} \mapsto (\mathbf{E})_{i,j} \sqrt{\lambda_1 \left(\mathbf{W}_{\mathrm{L^*a^*b^*}}\right)_{i,j}^2 + \lambda_2 \left(\mathbf{W}_{\mathrm{var}}\right)_{i,j}^2},$$

and $\iota_{C_{[0,1]}^{\mathbf{E}_{\mathrm{gvn}}}}$ and $\iota_{C_{\varepsilon}^{\mathbf{E}_{\mathrm{gvn}}}}$ are the indicator functions[5] of $C_{[0,1]}^{\mathbf{E}_{\mathrm{gvn}}}$ and $C_{\varepsilon}^{\mathbf{E}_{\mathrm{gvn}}}$, respectively. Now let

$$f : \mathbb{R}^{n_v \times n_h} \to [0, \infty] : \mathbf{E} \mapsto \tfrac{1}{2}\left\|\Omega\left(\mathbf{E}\right)\right\|_F^2 + \iota_{C_{[0,1]}^{\mathbf{E}_{\mathrm{gvn}}}}(\mathbf{E}), \tag{7}$$

$$\Lambda : \mathbb{R}^{n_v \times n_h} \to \mathbb{R}^{4N \times 3} \times \mathbb{R}^{n_v \times n_h} : \mathbf{E} \mapsto \big(\Phi(\mathbf{E}), \mathbf{E}\big), \tag{8}$$

$$g : \mathbb{R}^{4N \times 3} \times \mathbb{R}^{n_v \times n_h} \to [0, \infty] : (\mathbf{Z}_1, \mathbf{Z}_2) \mapsto \|\mathbf{Z}_1\|_* + \iota_{C_{\varepsilon}^{\mathbf{E}_{\mathrm{gvn}}}}(\mathbf{Z}_2). \tag{9}$$

Then, (6) is reduced to (1), so that we can utilize the ADMM for solving (6). The detail of the algorithm is shown in Algorithm 1, where I denotes the identity operator, and $(\cdot)^*$ stands for the adjoint of $(\cdot)$. Its implementation is summarized in Remark 3.1. Since a solution of (6) obtained by Algorithm 1 may consist of values between 0 and 1, we finally binarize it using threshold 0.5.

Remark 3.1. (Implementation of Algorithm 1)

- To compute the first step obtained by substituting (7) and (8) to (2), we require to solve the following zero-inclusion problem: find $\mathbf{E}$ s.t.[6]

$$\mathbf{0} \in (\Omega^* \circ \Omega + \rho\Lambda^* \circ \Lambda)(\mathbf{E}) + \partial\iota_{C_{[0,1]}^{\mathbf{E}_{\mathrm{gvn}}}}(\mathbf{E}) - \rho\Lambda^*\big(\mathbf{Y}^{(k)} - \tfrac{1}{\rho}\mathbf{\Theta}^{(k)}\big). \tag{10}$$

[5]For a given nonempty convex set C, the indicator function ι_C is defined by $\iota_C(\mathbf{X}) := 0$, if $\mathbf{X} \in C$; ∞, otherwise. The proximity operator of ι_C is equivalent to the *metric projection* onto C, i.e., $\mathrm{prox}_{\gamma\iota_C}(\mathbf{X}) = \arg\min_{Y\in C} \|\mathbf{X} - \mathbf{Y}\| =: P_C(\mathbf{X})$ $(\forall\gamma \in \mathbb{R}_{++})$.

[6]The subdifferential of a proper lower semicontinuous function f on $\mathcal{X}$ is defined by the following set-valued operator:

$$\partial f : \mathbf{x} \mapsto \{\mathbf{u} \in \mathcal{X} \mid (\forall \mathbf{y} \in \mathcal{X}) \; \langle \mathbf{y} - \mathbf{x}, \mathbf{u}\rangle + f(\mathbf{x}) \le f(\mathbf{y})\}.$$

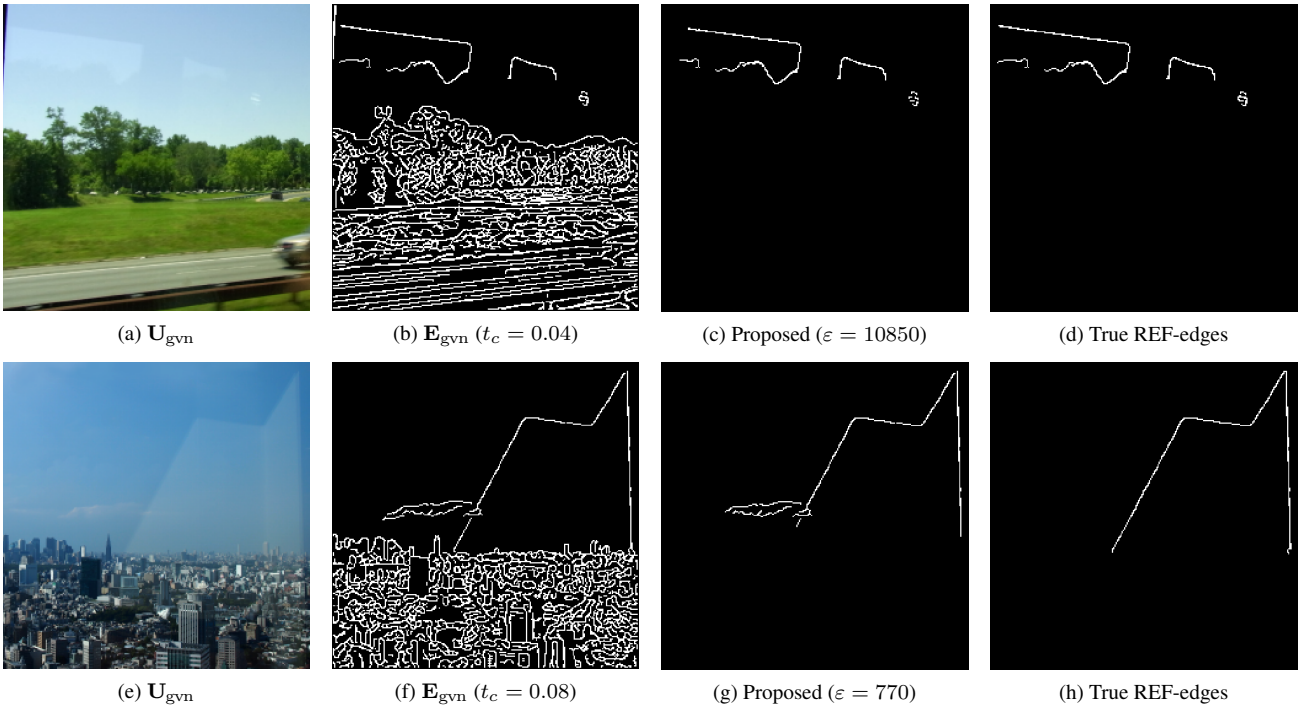

(a) $\mathbf{U}_{\mathrm{gvn}}$ (b) $\mathbf{E}_{\mathrm{gvn}}$ ($t_c = 0.04$) (c) Proposed ($\varepsilon = 10850$) (d) True REF-edges

(e) $\mathbf{U}_{\mathrm{gvn}}$ (f) $\mathbf{E}_{\mathrm{gvn}}$ ($t_c = 0.08$) (g) Proposed ($\varepsilon = 770$) (h) True REF-edges

Fig. 3: The results on the proposed method using real-world images: (c) and (g) show that our proposed method achieves an accurate estimation of REF-edges close to true REF-edges which are extracted manually from $\mathbf{E}_{\mathrm{gvn}}$.

Fortunately, the linear operators Ω and Λ are simply the entry-wise multiplication, and the set $C_{[0,1]}^{\mathbf{E}_{\mathrm{gvn}}}$ expresses the product of the closed intervals defined in (5). Hence, the inclusion problem can be solved with respect to each entry.[7] Consequently, the solution of (2) can be calculated as step 4 in Algorithm 1, where $P_{C_{[0,1]}^{\mathbf{E}_{\mathrm{gvn}}}} : \mathbb{R}^{n_v \times n_h} \to \mathbb{R}^{n_v \times n_h}$ is the metric projection onto $C_{[0,1]}^{\mathbf{E}_{\mathrm{gvn}}}$ given by

$$P_{C_{[0,1]}^{\mathbf{E}_{\mathrm{gvn}}}} : (\mathbf{E})_{i,j} \mapsto \begin{cases} 0 & \text{if } \big((\mathbf{E}_{\mathrm{gvn}})_{i,j} = 0\big) \vee \big((\mathbf{E})_{i,j} < 0\big), \\ (\mathbf{E})_{i,j} & \text{if } \big((\mathbf{E}_{\mathrm{gvn}})_{i,j} = 1\big) \wedge \big(0 \leq (\mathbf{E})_{i,j} \leq 1\big), \\ 1 & \text{if } \big((\mathbf{E}_{\mathrm{gvn}})_{i,j} = 1\big) \wedge \big((\mathbf{E})_{i,j} > 1\big). \end{cases}$$

- The computation of (3) can be decoupled with respect to the proximity operators of each function in (9). The proximity operator of $\|\cdot\|_*$ is given by

$$\mathrm{prox}_{\gamma\|\cdot\|_*} : \mathbb{R}^{4N \times 3} \to \mathbb{R}^{4N \times 3} : \mathbf{M} \mapsto \mathbf{P}\widetilde{\mathbf{\Sigma}}\mathbf{Q}^\top,$$

where the matrices $\mathbf{P}$ and $\mathbf{Q}$ are the left-singular and right-singular matrices of $\mathbf{M}$, and the matrix $\widetilde{\mathbf{\Sigma}}$ contains the singular values shrank by γ on its main diagonal and 0's elsewhere. Meanwhile, the proximity operator of $\iota_{C_\varepsilon^{\mathbf{E}_{\mathrm{gvn}}}}$ can be calculated by a fast ℓ_1-ball projection technique [13].

[7] The inclusion problem in (10) with respect to each entry is equivalent to find $(\mathbf{E})_{i,j}$ s.t. $0 \in \alpha_{i,j}(\mathbf{E})_{i,j} + \partial\iota_{C_{[0,1]}^{(\mathbf{E}_{\mathrm{gvn}})_{i,j}}}\big((\mathbf{E})_{i,j}\big) - \beta_{i,j}$, where $\alpha_{i,j} \in \mathbb{R}_{++}$ is the weight corresponding to the (i,j)-th multiplication regarding $(\Omega^* \circ \Omega + \rho\Lambda^* \circ \Lambda)$, $\beta_{i,j} := \big(\rho\Lambda^*(\mathbf{Y}^{(k)} - \frac{1}{\rho}\mathbf{\Theta}^{(k)})\big)_{i,j}$, and $C_{[0,1]}^{(\mathbf{E}_{\mathrm{gvn}})_{i,j}}$ is the (i,j)-th closed interval. Since $\partial\iota_{C_{[0,1]}^{(\mathbf{E}_{\mathrm{gvn}})_{i,j}}}\big((\mathbf{E})_{i,j}\big)$ over $\alpha_{i,j}$ equals $\partial\iota_{C_{[0,1]}^{(\mathbf{E}_{\mathrm{gvn}})_{i,j}}}\big((\mathbf{E})_{i,j}\big)$, we obtain

$$(\mathbf{E})_{i,j} = P_{C_{[0,1]}^{(\mathbf{E}_{\mathrm{gvn}})_{i,j}}}(\alpha_{i,j}/\beta_{i,j}).$$

4. EXAMPLES

We examine the effectiveness of the proposed method using real-world images containing reflections. In Algorithm 1, we generate an initial edge image $\mathbf{E}_{\mathrm{gvn}}$ using the Canny's edge detector [14], which is a well-known edge detector, with threshold t_c to each RGB channel of $\mathbf{U}_{\mathrm{gvn}}$. Then, we apply Algorithm 1 to the images, where $n_v = n_h = 250$, $r = 15$, $\rho = 1$, $\lambda_1 = 100$, $\lambda_2 = 30$, and the stopping criterion is $\|\mathbf{E}^{(k+1)} - \mathbf{E}^{(k)}\|_F \leq 10^{-4}$. The weights λ_1 and λ_2 are determined according to the strength of reflections and frequency of color change.

Results are shown in Fig. 3 (including given color images, initial edge images, the estimate by using the proposed method, and true REF-edge images). The use of the proposed method achieves a sufficient extraction of REF-edges without containing almost all non-REF-edges, so that the resulting estimate is very close to the true REF-edge images that are manually detected.

5. CONCLUDING REMARKS

We have proposed to detect edges of reflections, i.e., REF-edges, from a single image via convex optimization. The proposed method exploits the REF-linearity, small color differences, and small variance of gradients characterizing REF-edges in our optimization formulation. The optimization problem is solved by the ADMM. We have illustrated that the proposed method detects REF-edges effectively from real-world images containing reflections.

6. REFERENCES

[1] H. Farid and H. Adelson, "Separating reflections from images by use of independent component analysis," *J. Opt. Soc. Amer.*, vol. 16, no. 9, pp. 2136–2145, 1999.

[2] Y. Y. Schechner, J. Shamir, and N. Kiryati, "Polarization and statistical analysis of scenes containing a semireflector," *J. Opt. Soc. Amer.*, vol. 17, no. 2, pp. 276–284, 2000.

[3] A. Levin and Y. Weiss, "User assisted separation of reflections from a single image using a sparsity prior," *IEEE Trans. Pattern Analysis and Machine Intelligence*, vol. 29, no. 9, pp. 1647–1654, 2007.

[4] N. Kong, Y. Tai, and S. Shin, "High-quality reflection separation using polarized images," *IEEE Trans. Image Processing*, vol. 20, no. 12, pp. 3393–3405, 2011.

[5] Y. Li and M. Brown, "Exploiting reflection change for automatic reflection removal," in *Proc. IEEE ICCV*, 2013.

[6] X. Ma and W. E. L. Grimson, "Edge-based rich representation for vehicle classification," in *Proc. IEEE ICCV*, 2005, vol. 2, pp. 1185–1192.

[7] M. A. Ahmed, F. Pitie, and A. Kokaram, "Reflection detection in image sequences," in *Proc. IEEE CVPR*, 2011, pp. 705–712.

[8] M. Elgharib, F. Pitie, A. Kokaram, and V. Saligrama, "User-assisted reection detection and feature point tracking," in *European Conference on Visual Media Production (CVMP)*, 2013.

[9] D. Gabay and B. Mercier, "A dual algorithm for the solution of nonlinear variational problems via finite element approximation," *Computers & Mathematics with Applications*, vol. 2, no. 1, pp. 17–40, 1976.

[10] M. Fazel, *Matrix rank minimization with applications*, Ph.D. thesis, Stanford University, 2002.

[11] J. Eckstein and D. P. Bertsekas, "On the douglas-rachford splitting method and the proximal point algorithm for maximal monotone operators," *Mathematical Programming*, vol. 55, no. 1-3, pp. 293–318, 1992.

[12] S. Ono and I. Yamada, "A convex regularizer for reducing color artifact in color image recovery," in *Proc. IEEE CVPR*, 2013, pp. 1775–1781.

[13] J. Duchi, S. Shalev-Shwartz, Y. Singer, and T. Chandra, "Efficient projections onto the l 1-ball for learning in high dimensions," in *Proc. ICML*, 2008, pp. 272–279.

[14] J. Canny, "A computational approach to edge detection," *IEEE Trans. Pattern Analysis and Machine Intelligence*, vol. 8, no. 6, pp. 679–698, 1986.